Supplementary Information

High-Entropy Strategies Afford Transition Metal Perovskite Oxides with Enhanced Low-Temperature NO_x Removal Efficiency

Xuan Zhang,[a,b] Dequan Jiang,[a] Shenghui Han,[a] Wanli Yi,[a] Jianwen Su,[a] Song Gao,[a,*] Yonggang Wang,[a,*] Ruqiang Zou[a]

[a]State Key Laboratory of Advanced Waterproof Materials, School of Materials Science and Engineering, Peking University, Beijing, 100871, PR China.

[b]Beijing Key Laboratory for Solid Waste Utilization and Management, Peking University, Beijing, 100871, PR China

*Corresponding author: gaosong198600@pku.edu.cn (S.G.); ygw@pku.edu.cn (Y.W.)

1. Sample preparation and characterizations.

Powder samples of $LaBO_3$ (B is the transition metal oxides, Co, Mn, Fe, Ni, Cr, Al, Mo, W, the metal source was selected for the B site in ABO_3 because they have similar six-coordination ionic radii) were synthesized using the citric acid sol-gel method. A certain amount of metal nitrates ($La(NO_3)_3 \cdot 6H_2O$, $Mn(NO_3)_2$, $Co(NO_3)_2 \cdot 6H_2O$, $Ni(NO_3)_2 \cdot 6H_2O$, $Cr(NO_3)_3 \cdot 9H_2O$, $Al(NO_3)_3 \cdot 9H_2O$, $Fe(NO_3)_2 \cdot 9H_2O$, $Na_2WO_4 \cdot 2H_2O$, $C_4H_4NNbO_9.nH_2O$) were dissolved in deionized water and citric acid and ethylene glycol were then added into the above solution and stirred for 3 h at 150 °C. When the above solution became viscous precursors, the stirring process was stopped. Subsequently, the viscous precursors were dried overnight at 200°C and finally calcinated at 700 °C in air atmosphere for 6 hours. The resulting samples were marked in the following table.

Samples synthesized in this work.

	Sample	La	Co	Mn	Fe	Ni	Cr	Al	
1	$La(Co_{0.2}Mn_{0.2}Fe_{0.2}Ni_{0.2}Cr_{0.2})O_{3-\delta}$	1.0	0.2	0.2	0.2	0.2	0.2	**NO**	HEP-no-Al
2	$La(Co_{0.2}Mn_{0.2}Fe_{0.2}Ni_{0.2}Al_{0.2})O_{3-\delta}$	1.0	0.2	0.2	0.2	0.2	**NO**	0.2	HEP-no-Cr
3	$La(Co_{0.2}Mn_{0.2}Fe_{0.2}Al_{0.2}Cr_{0.2})O_{3-\delta}$	1.0	0.2	0.2	0.2	**NO**	0.2	0.2	HEP-no-Ni
4	$La(Co_{0.2}Mn_{0.2}Ni_{0.2}Al_{0.2}Cr_{0.2})O_{3-\delta}$	1.0	0.2	0.2	**NO**	0.2	0.2	0.2	HEP-no-Fe
5	$La(Co_{0.2}Fe_{0.2}Ni_{0.2}Al_{0.2}Cr_{0.2})O_{3-\delta}$	1.0	0.2	**NO**	0.2	0.2	0.2	0.2	HEP-no-Mn
6	$La(Mn_{0.2}Fe_{0.2}Ni_{0.2}Al_{0.2}Cr_{0.2})O_{3-\delta}$	1.0	**NO**	0.2	0.2	0.2	0.2	0.2	HEP-no-Co
	Sample	**La**	**Co**	**Mn**	**Fe**	**Ni**	**Cr**	**Mo**	**W**
7	$La(Co_{0.2}Mn_{0.2}Fe_{0.2}Ni_{0.2}Cr_{0.2})O_{3-\delta}$	1.0	0.2	0.2	0.2	0.2	0.2	**NO**	**NO** HEP-Cr
8	$La(Co_{0.2}Mn_{0.2}Fe_{0.2}Ni_{0.2}Mo_{0.2})O_{3-\delta}$	1.0	0.2	0.2	0.2	0.2	**NO**	0.2	**NO** HEP-Mo
9	$La(Co_{0.2}Mn_{0.2}Fe_{0.2}Ni_{0.2}W_{0.2})O_{3-\delta}$	1.0	0.2	0.2	0.2	0.2	**NO**	**NO**	0.2 HEP-W

X-ray diffraction (XRD) patterns of as-prepared samples were collected by a powder X-ray diffractometer (Rigaku Dmax-2400, RIGAKU, Japan) with Cu-Kα target. The textural properties of as-prepared samples were investigated using a nitrogen adsorption apparatus (ASAP2020, Micromeritics, US) at 77K. Specific surface area, pore volume and pore size distribution were obtained by Brunauer–Emmett–Teller (BET), single point and Barret–Joyner–Halenda (BJH) methods, respectively. Surface morphologies of the as-prepared samples were analyzed using a field emission scanning electron microscope (Merlin Compact, ZEISS, Germany) operating at 10 kV. Transmission electron microscopy (TEM) images of as-prepared samples were screened on a transmission electron microscope (JEM-2100F, JEOL, Japan) operating at 200 kV. The

surface chemical species of the as-prepared samples were characterized by X-ray photoelectron spectroscopy (AXIS Supra, Kratos Analytical Ltd, UK) with Al Kα radiation. H_2 temperature-programmed reduction (H_2-TPR) and NH3 temperature-programmed desorption (NH_3-TPD) experiments were carried out on a chemisorption analyzer (Chem-BET Pulsar TPR/TPD, Quanta-chrome, US). The samples were firstly pretreated under a high purified N_2 stream at 400 °C for 1 h to remove physiosorbed water and other impurities. Subsequently, a stream of NH_3/N_2 (1 vol% NH_3) was passed over the samples at room temperature, followed by purging with N_2 for 30 minutes. The desorption of NH_3 was studied by heating pre-adsorbed samples, and the spectra were recorded at stepped target temperatures by eliminating the corresponding background reference.

NH_3-SCR activity measurements. The catalytic performances were tested in a fixed-bed NH_3-SCR quartz reactor (6 mm of internal diameter) in the temperature range from 90 to 390 °C with a GHSV of 15000 h^{-1}. The reaction gas mixture consisted of 500 ppm NH_3, 3% O_2 and N_2 in balance. Firstly, 200 mg catalyst was pretreated with N_2 at 200 °C for 30 minutes to eliminate physiosorbed water. The concentrations of NO and NO_2 were obtained through a flue gas analyzer (Testo 350 Pro, Testo, Germany) when the catalytic reaction substantially reached a steady state at every target temperature. NO_x conversion efficiency was calculated according to the following formula:

$$NO_x\ conversion\ rate = \left(1 - \frac{[NO_x]_{out}}{[NO_x]_{in}}\right) \times 100\%, \quad ([NO_x]=[NO]+[NO_2])$$

2. Supporting figures and tables.

Fig. S1 Lattice parameter (a and c) of HEP catalysts.

Fig. S2 Lattice Volume of HEP catalysts.

Fig. S3 N_2 adsorption and desorption curve and pore size distribution curve of $La(Co_{0.2}Mn_{0.2}Fe_{0.2}Ni_{0.2}Cr_{0.2})O_{3-\delta}$.

Fig. S4 N_2 adsorption and desorption curve and pore size distribution curve of $La(Co_{0.2}Mn_{0.2}Fe_{0.2}Al_{0.2}Cr_{0.2})O_{3-\delta}$.

Fig. S5 N_2 adsorption and desorption curve and pore size distribution curve of $La(Co_{0.2}Mn_{0.2}Ni_{0.2}Al_{0.2}Cr_{0.2})O_{3-\delta}$.

Fig. S6 N_2 adsorption and desorption curve and pore size distribution curve of $La(Mn_{0.2}Fe_{0.2}Ni_{0.2}Al_{0.2}Cr_{0.2})O_{3-\delta}$.

Fig. S7 N_2 adsorption and desorption curve and pore size distribution curve of $La(Co_{0.2}Mn_{0.2}Fe_{0.2}Ni_{0.2}Al_{0.2})O_{3-\delta}$.

Fig. S8 N_2 adsorption and desorption curve and pore size distribution curve of $La(Co_{0.2}Mn_{0.2}Ni_{0.2}Al_{0.2}Cr_{0.2})O_{3-\delta}$.

Fig. S9 TEM of $La(Co_{0.2}Mn_{0.2}Fe_{0.2}Ni_{0.2}Cr_{0.2})O_{3-\delta}$.

Fig. S10 TEM of $La(Co_{0.2}Mn_{0.2}Fe_{0.2}Ni_{0.2}Mo_{0.2})O_{3-\delta}$.

Fig. S11 The Surface valence states of the A and B-site elements.

Fig. S12 H_2-TPR spectra of HEP-Cr\Mo\W catalysts.

Table S1 BET surface area and pore size of HEP catalysts.

Table S2 XPS data for all the samples.

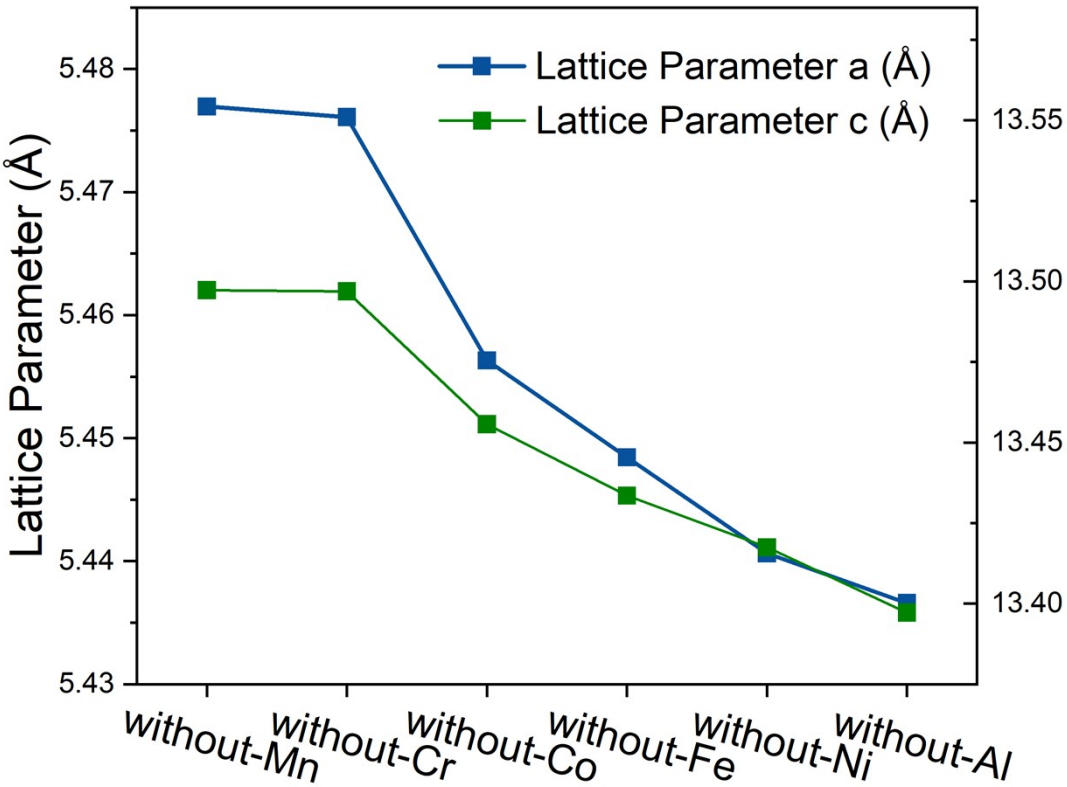

Fig. S1 Lattice parameter (a and c) of HEP catalysts.

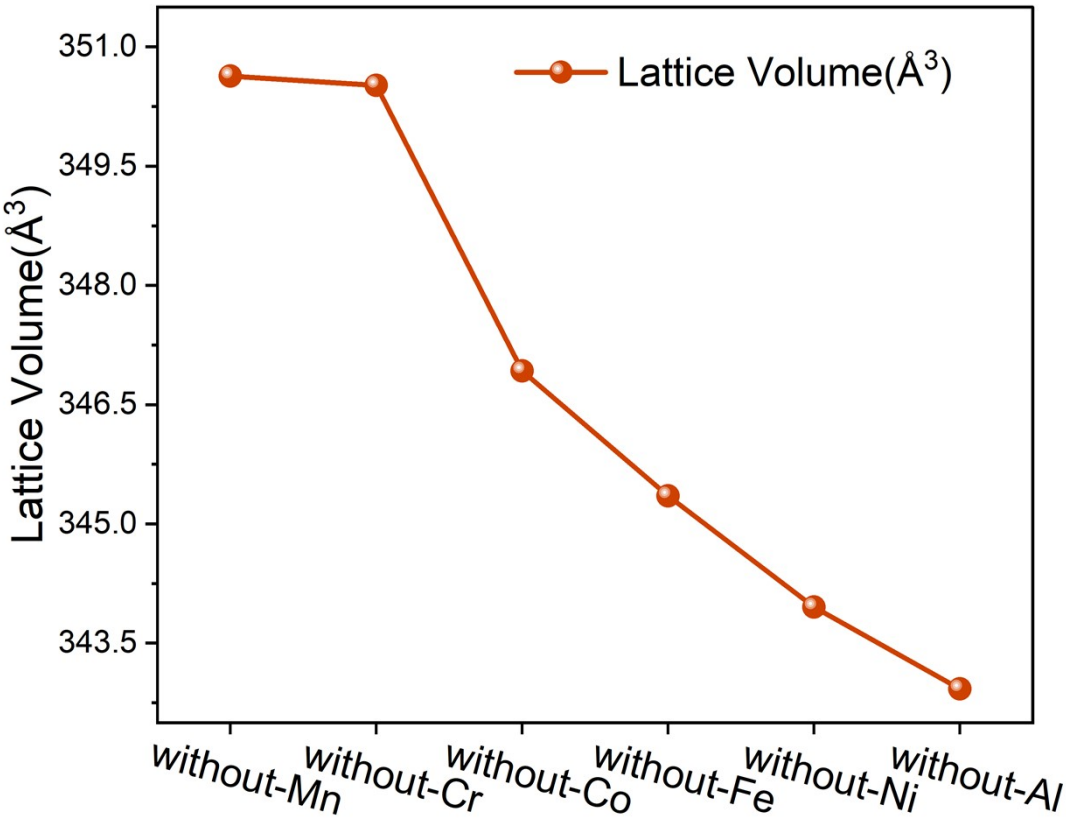

Fig. S2 Lattice Volume of HEP catalysts.

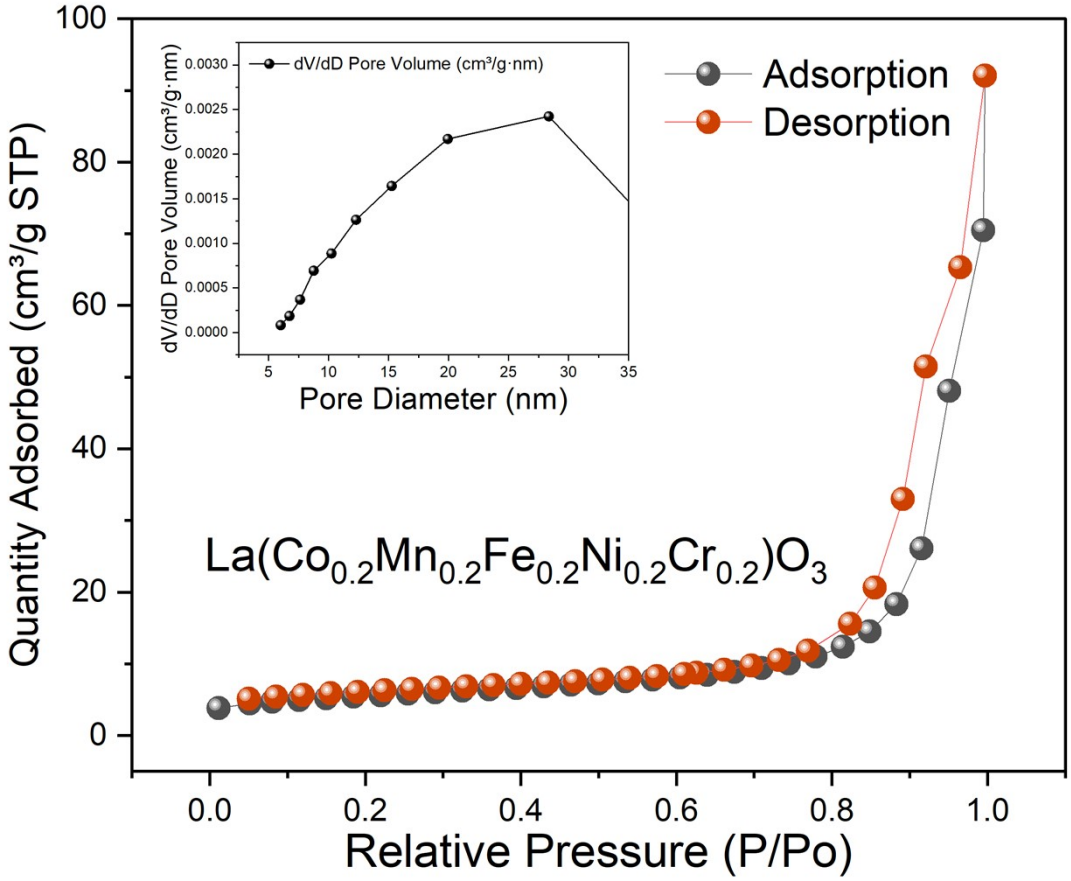

Fig. S3 N_2 adsorption and desorption curve and pore size distribution curve of $La(Co_{0.2}Mn_{0.2}Fe_{0.2}Ni_{0.2}Cr_{0.2})O_{3-\delta}$.

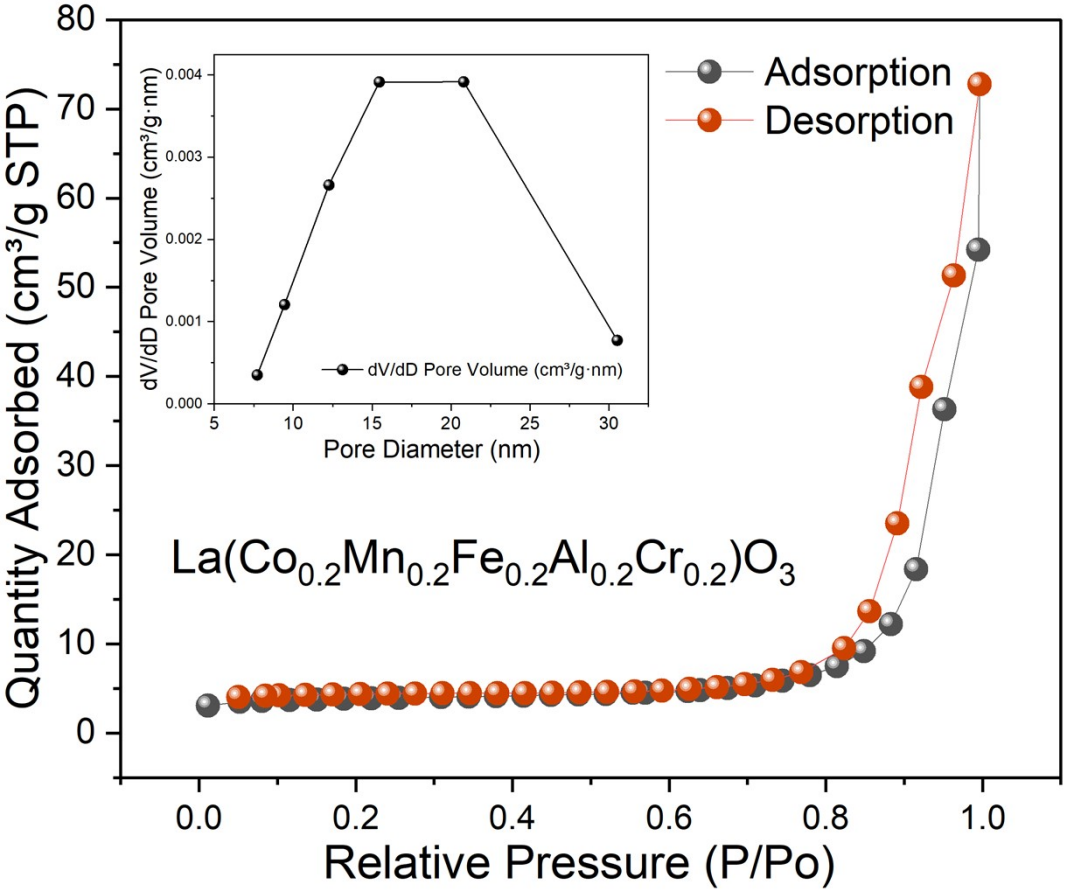

Fig. S4 N_2 adsorption and desorption curve and pore size distribution curve of $La(Co_{0.2}Mn_{0.2}Fe_{0.2}Al_{0.2}Cr_{0.2})O_{3-\delta}$.

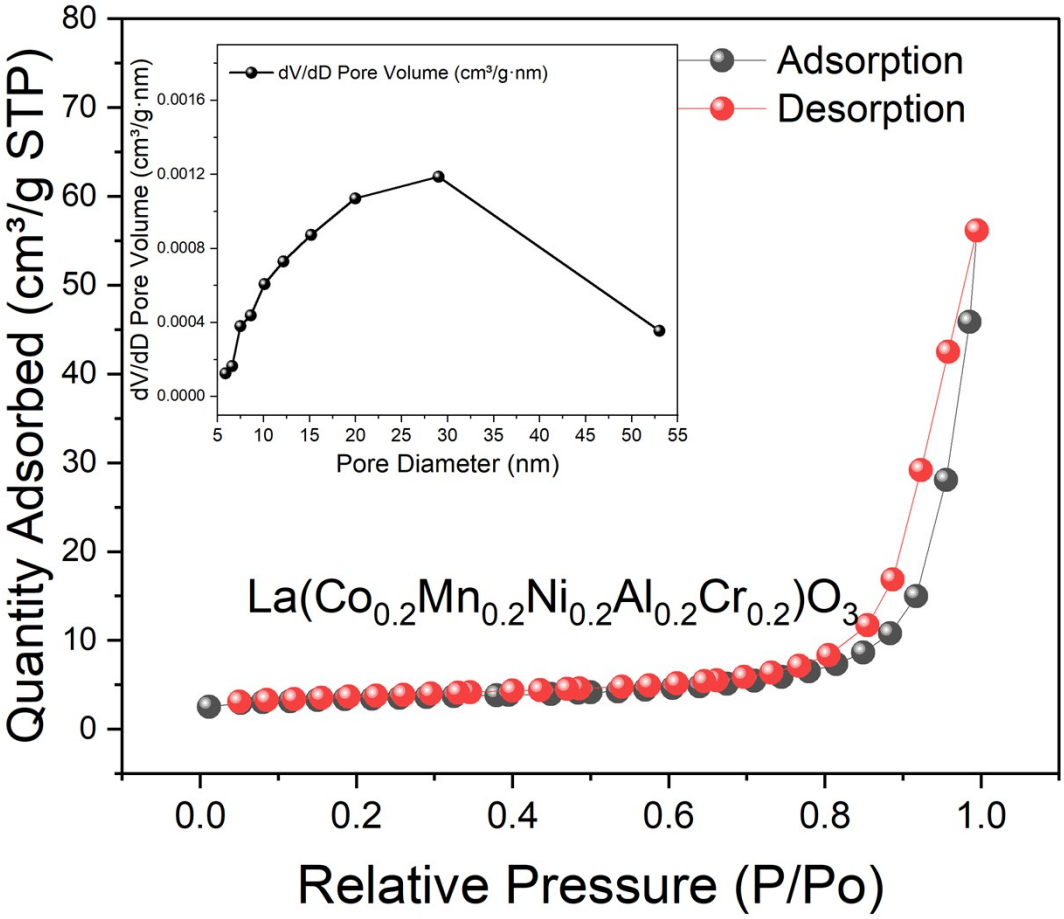

Fig. S5 N_2 adsorption and desorption curve and pore size distribution curve of $La(Co_{0.2}Mn_{0.2}Ni_{0.2}Al_{0.2}Cr_{0.2})O_{3-\delta}$.

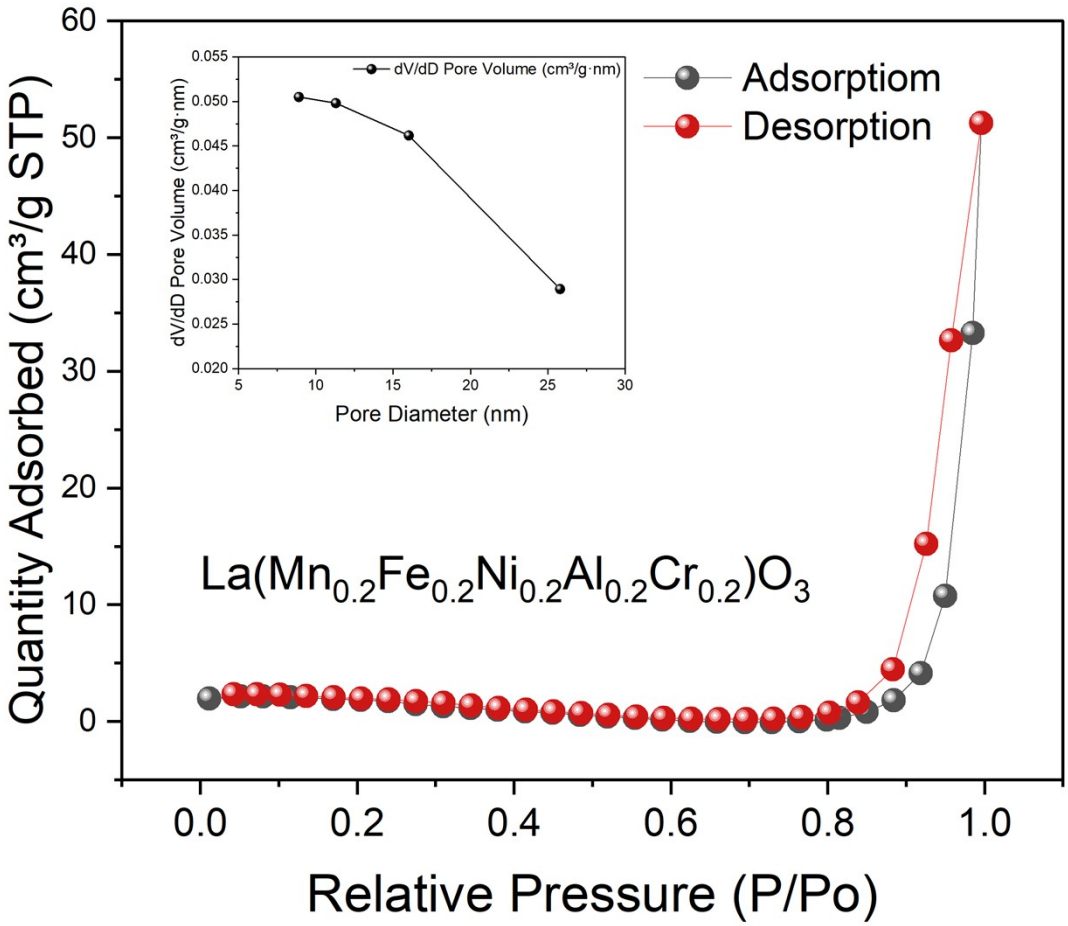

Fig. S6 N_2 adsorption and desorption curve and pore size distribution curve of $La(Mn_{0.2}Fe_{0.2}Ni_{0.2}Al_{0.2}Cr_{0.2})O_{3-\delta}$.

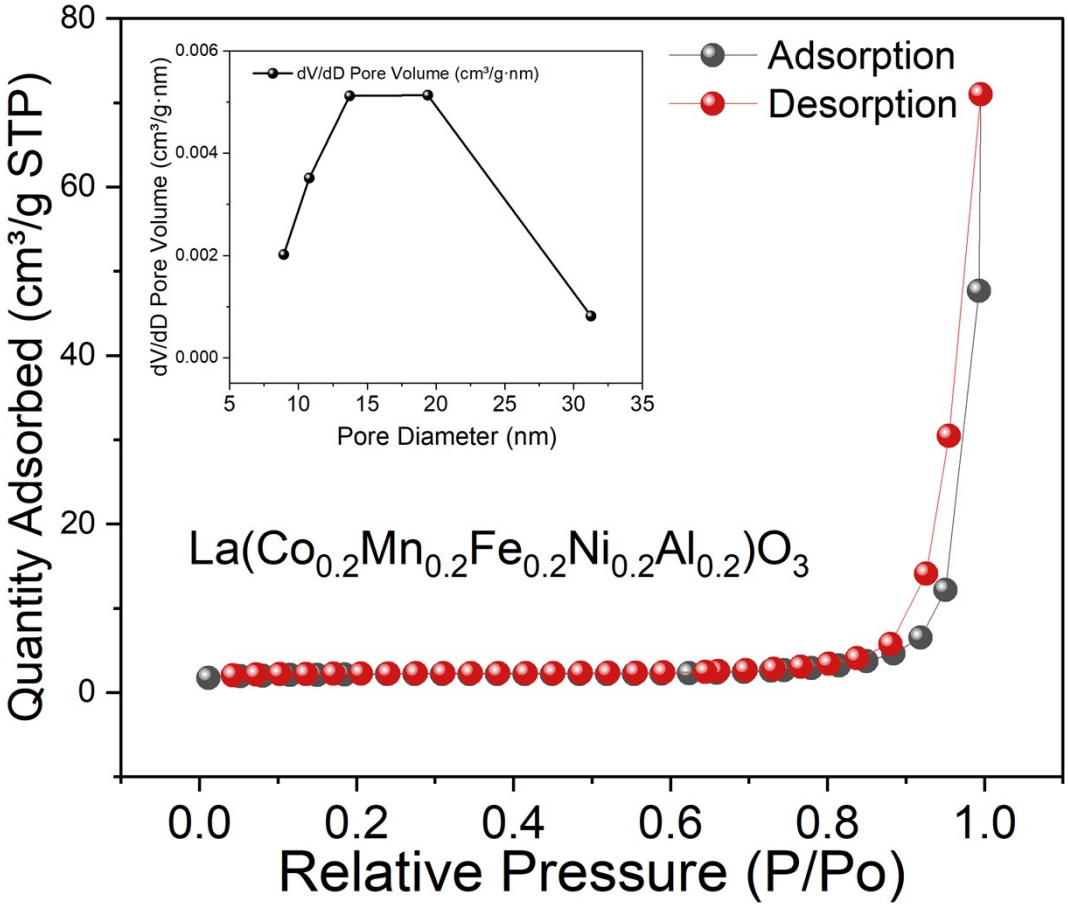

Fig. S7 N_2 adsorption and desorption curve and pore size distribution curve of $La(Co_{0.2}Mn_{0.2}Fe_{0.2}Ni_{0.2}Al_{0.2})O_{3-\delta}$.

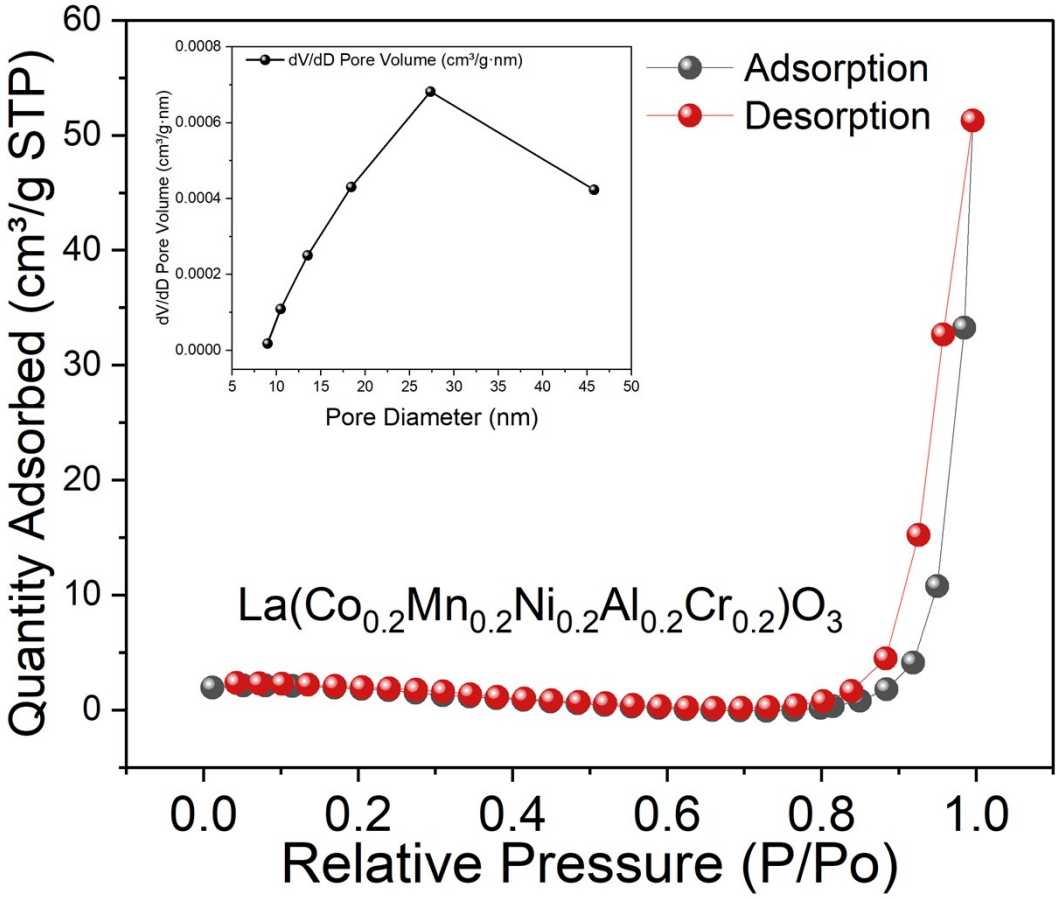

Fig. S8 N_2 adsorption and desorption curve and pore size distribution curve of $La(Co_{0.2}Mn_{0.2}Ni_{0.2}Al_{0.2}Cr_{0.2})O_{3-\delta}$.

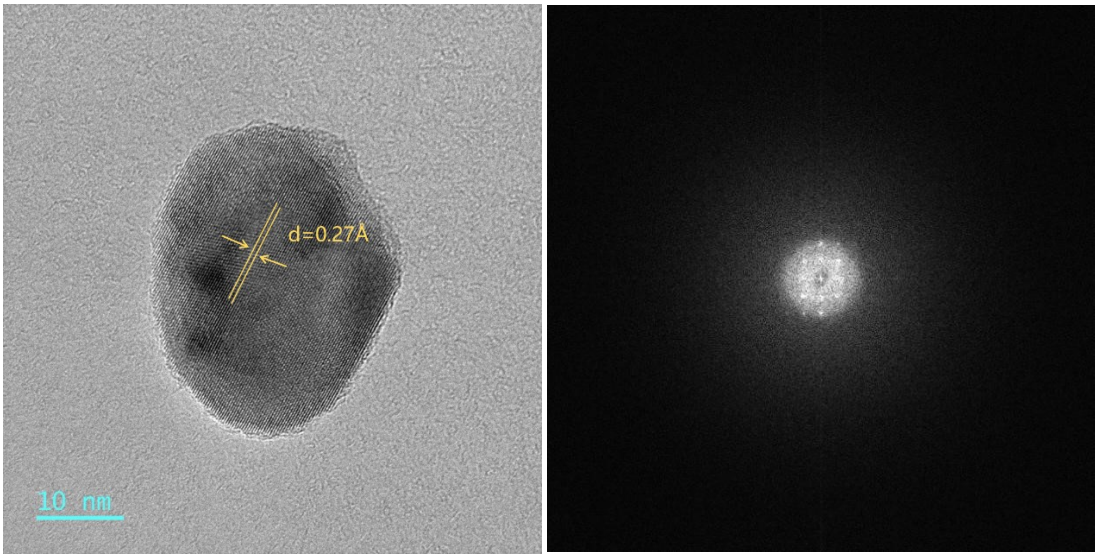

Fig. S9 TEM of $La(Co_{0.2}Mn_{0.2}Fe_{0.2}Ni_{0.2}Cr_{0.2})O_{3-\delta}$.

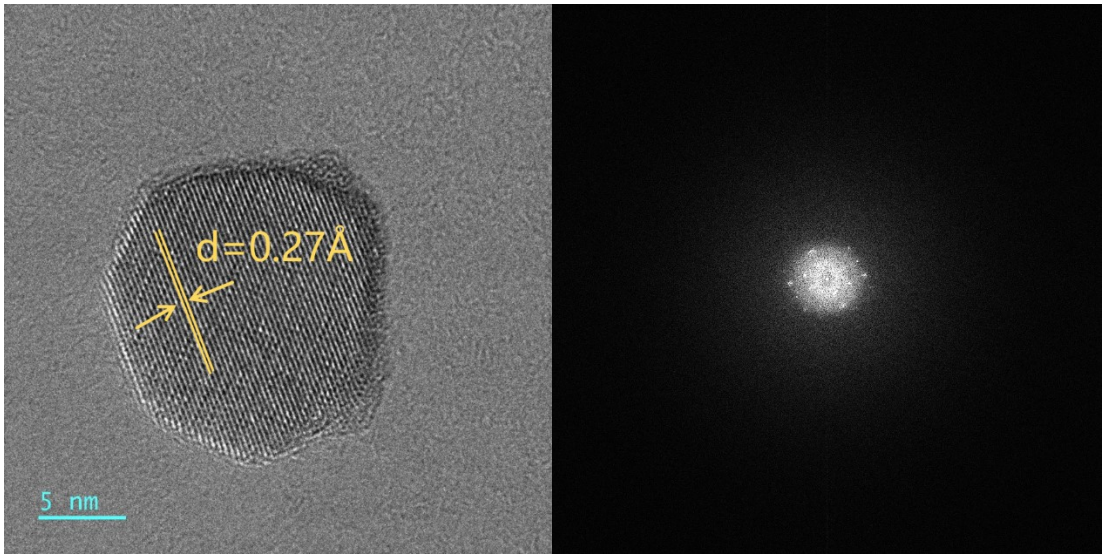

Fig. S10 TEM of $La(Co_{0.2}Mn_{0.2}Fe_{0.2}Ni_{0.2}Mo_{0.2})O_{3-\delta}$.

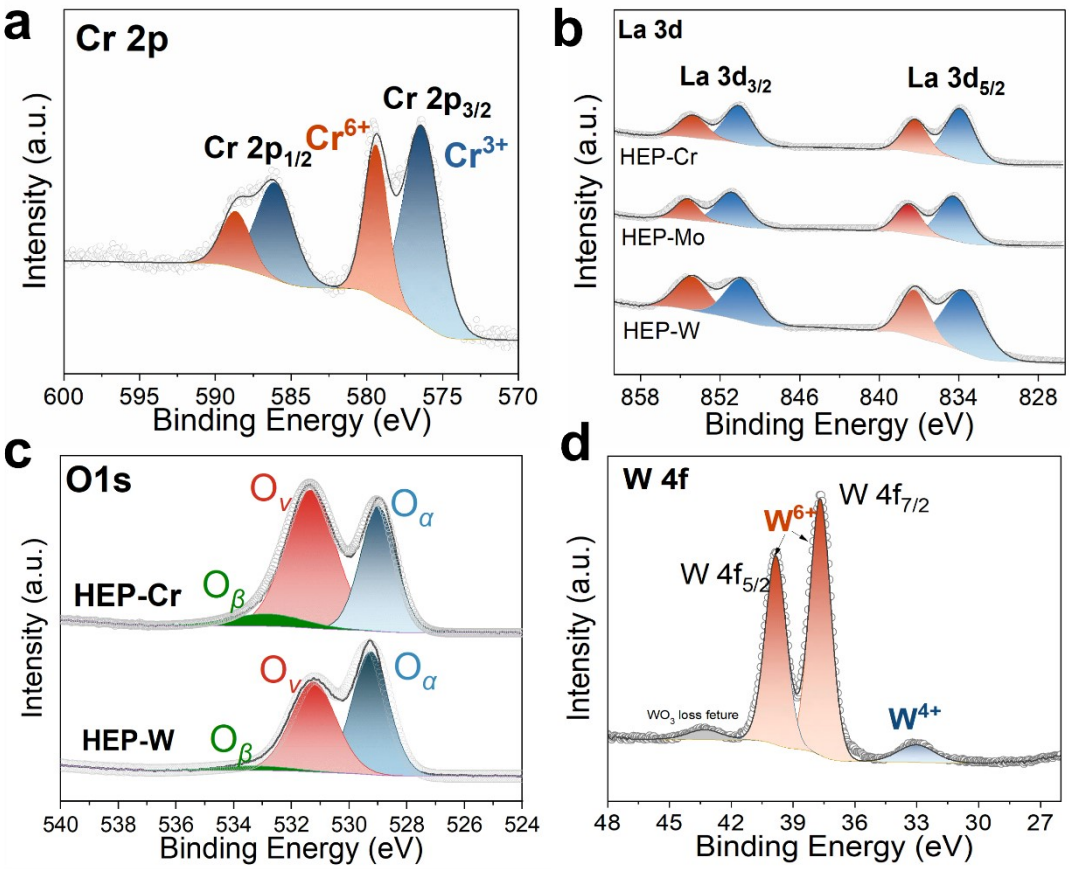

Fig. S11 The Surface valence states of the A and B-site elements.

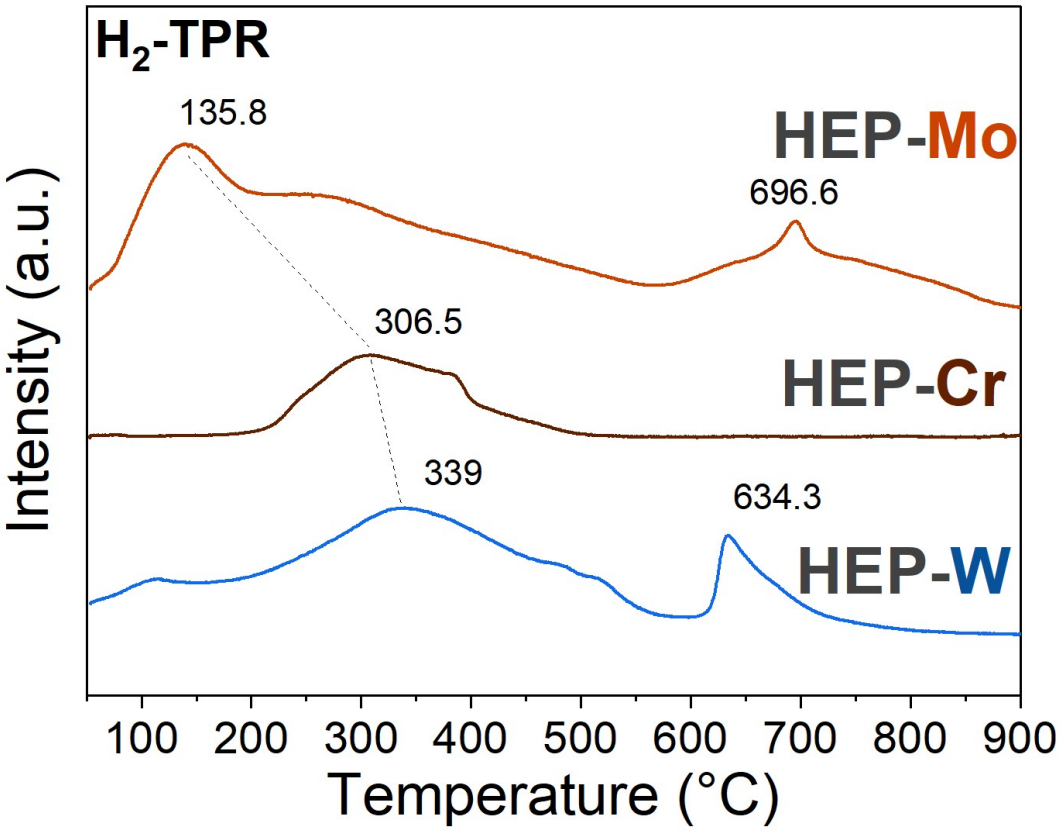

Fig. S12 H_2-TPR spectra of HEP-Cr\Mo\W catalysts.

Table S1 BET surface area and pore size of HEP catalysts.

Catalysts	BET surface area (m^2/g)	Total pore volume (cm^3/g)	Average pore diameter (nm)
No-Al $La(Co_{0.2}Mn_{0.2}Fe_{0.2}Ni_{0.2}Cr_{0.2})O_{3-\delta}$	19.3728	0.1125	18.4441
No-Ni $La(Co_{0.2}Mn_{0.2}Fe_{0.2}Al_{0.2}Cr_{0.2})O_{3-\delta}$	14.6548	0.1004	18.7365
No-Fe $La(Co_{0.2}Mn_{0.2}Ni_{0.2}Al_{0.2}Cr_{0.2})O_{3-\delta}$	12.3265	0.0869	19.9404
No-Co $La(Mn_{0.2}Fe_{0.2}Ni_{0.2}Al_{0.2}Cr_{0.2})O_{3-\delta}$	8.0309	0.0505	22.7561
No-Cr $La(Co_{0.2}Mn_{0.2}Fe_{0.2}Ni_{0.2}Al_{0.2})O_{3-\delta}$	8.1617	0.0465	24.4184
No-Mn $La(Co_{0.2}Fe_{0.2}Ni_{0.2}Al_{0.2}Cr_{0.2})O_{3-\delta}$	6.2920	0.0558	21.3337

Table S2 XPS data for all the samples.

Catalysts	La^{3+}	Cr^{6+}/Cr^{3+}	Mn^{4+}/Mn^{3+}	Fe^{3+}/Fe^{2+}	Co^{3+}/Co^{2+}	Ni^{3+}/Ni^{2+}	Al^{3+}	O_{α}	O_{v}	O_{β}
No-Al $La(Co_{0.2}Mn_{0.2}Fe_{0.2}Ni_{0.2}Cr_{0.2})O_{3-\delta}$	100%	0.56	0.51	0.95	1.44	0.68	--	36.88	58.20	4.93
No-Ni $La(Co_{0.2}Mn_{0.2}Fe_{0.2}Al_{0.2}Cr_{0.2})O_{3-\delta}$	100%	0.54	0.37	0.83	1.37	--	1.0	36.14	56.30	7.55
No-Fe $La(Co_{0.2}Mn_{0.2}Ni_{0.2}Al_{0.2}Cr_{0.2})O_{3-\delta}$	100%	0.51	0.35	--	1.14	0.65	1.0	39.58	53.00	7.41
No-Co $La(Mn_{0.2}Fe_{0.2}Ni_{0.2}Al_{0.2}Cr_{0.2})O_{3-\delta}$	100%	0.46	0.34	0.75	--	0.57	1.0	45.65	50.64	3.72
No-Cr $La(Co_{0.2}Mn_{0.2}Fe_{0.2}Ni_{0.2}Al_{0.2})O_{3-\delta}$	100%	--	0.28	0.73	1.14	0.57	1.0	44.84	47.83	7.33
No-Mn $La(Co_{0.2}Fe_{0.2}Ni_{0.2}Al_{0.2}Cr_{0.2})O_{3-\delta}$	100%	0.37	--	0.49	0.92	0.50	1.0	49.86	45.56	4.57

120